Evaluating The Relationships Between Surface Roughness And Friction Behavior During Metal Forming

M. R. Stoudt
J. B. Hubbard
S. P. Mates
Materials Science & Engineering Laboratory
National Institute of Standards and Technology
Gaithersburg, MD 20899-8553, USA

D. E. Green
Mechanical Engineering Department
University of Windsor
Windsor, Ontario, N9B 3P4, Canada

ABSTRACT

The inhomogeneous distribution of surface asperities generated by deformation induces variability in the friction and initiates strain localizations during metal forming. The friction literature generally does not account for the strong influence localized variations in material properties have on the friction behavior. A prototype apparatus was developed that measures the friction behavior under simulated forming conditions and enables detailed characterization of the influences of the microstructure and the topographical conditions that occur under those conditions. The results demonstrate that the measurement system can resolve subtle real-time changes in the dynamic friction coefficient, and that a correlation could exist between the largest surface asperities and the largest variations in the measured friction coefficient.

INTRODUCTION

The property differences that exist between traditional automotive steel alloys and many of the new alloys designed to improve automotive fuel economy pose a significant challenge to our understanding of metal formability. The inhomogeneous surface roughening and variability in the deformation behavior [1-3] often initiate strain localizations that promote necking, tearing, or wrinkling in stamped metallic components.

During metal stamping, the flow of the work piece into the die cavity is usually controlled with a binder (holding) clamp and a drawbead. Appropriate drawbead shapes and clamping forces on the sheet stock have been effective in preventing wrinkling and tearing in the stamping [4]. However, deviations from the predicted deformation behavior around the drawbead or in the binder clamp may result in insufficient or excessive clamping forces that can increase wrinkling or tearing. Furthermore, the increased sensitivity to variations in alloying content and metallurgical processing conditions exhibited by many of the newer alloys cause inconsistencies in the metal properties that exacerbate the forming difficulties [5]. Recent studies have resulted in better drawbead designs [6], as well as in new approaches to locally monitor and control the clamping forces on the binder [7, 8]. While successful to some degree, these studies still heavily rely on the quality of the empirical friction data used in the finite element analysis (FEA) predictions.

Many investigators [9-12] have successfully measured frictional forces under a range of simulated metal forming conditions and a wealth of data is available in the literature. However, the literature also shows that the coefficients of friction are highly dependent upon the parameters used in the friction test (e.g., sliding time, indentation force, strain rate, and test environment) [13-15]. Traditional friction measurements tend to strictly focus on the mechanics of friction and do not account for the dynamic response of the material during the deformation process. Most of these data do not account for the strong influences that variations in metallurgical conditions have on the material properties. For this reason, the friction values selected for an FEA simulation may not be entirely representative of the actual metal behavior under those particular conditions. Since the traditional approaches cannot provide the essential data, there is a need for new approaches that a) evaluate both the static and the dynamic properties for the materials of

interest, and b) provide a more broad-based understanding of the relationships between the friction behavior and the microstructural variations that affect the properties during metal forming.

A prototype friction testing apparatus is being developed as part of a test protocol that produces friction data under a wide range of loading and strain rate conditions in response to this need. The principal advantage of this protocol is that it enables direct assessment of the relative influence of metallurgical variables, such as composition, grain size and orientation effects, strengthening mechanisms, slip homogeneity, as well as changes in the microstructures that are produced under conditions closely emulating those encountered in industrial forming operations. These measurements can then be used to guide the development of improved finite element models that predict the shape of the formed part after each forming operation. This particular study focuses on the suitability of the design to produce and measure the friction under different surface conditions.

EXPERIMENTAL

MATERIAL- Hot-dipped galvanized DQSK steel is a relatively common automotive alloy that demonstrates good formability so it was selected as the material for this evaluation. The steel sheet had an initial thickness of 1 mm with a zinc coating of approximately 170 μm. Metallographic analysis revealed that the average grain size of the DQSK steel was 20 μm ± 7 μm. This is substantially smaller than the microstructure observed in the zinc layer shown in Figure 1.
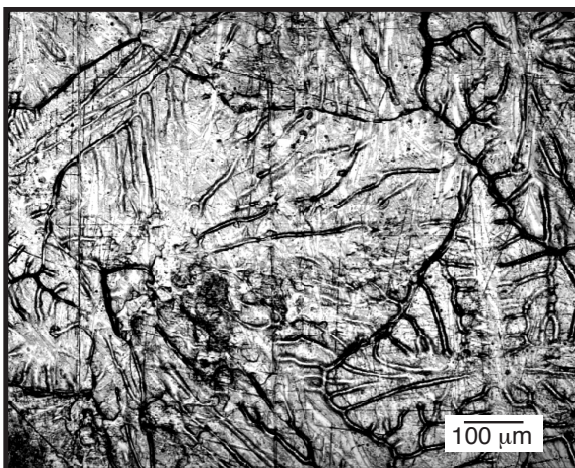

100 μm

Figure 1. SLCM image of the surface of the hot-dipped galvanized DQSK steel in the as-received condition. Note that the grain structure of the zinc layer is substantially different from that of the underlying steel.

Pre-strained channel sections were provided for these experiments by IRDI. An A/SP channel draw die formed each blank into an open-ended channel section (Figure

2). During the forming of the channel, the floating binder maintained a constant pressure against the upper die by means of pressure pins that were connected to a pressure cushion positioned beneath the press bolster. Four "kiss blocks" mounted on the binder ensured a constant clearance between the binder and the upper die. The material on either side of the central punch then flowed through a drawbead and over the die entry radius (inserts B & C in Figure 3). The drawbeads used for the straining had the following configuration: The male beads were round with a 4.0 mm profile radius. The female insert had a width of 10.8 mm, and a profile radius of 4.0 mm. The horizontal clearance on each side of the male bead was 1.4 mm and the vertical clearance between the binder and the upper die was equivalent to material thickness plus approximately 0.4 mm. The die entry radius was 12.0 mm. Prior to forming channel sections in the draw die, blanks were sheared lengthways across the width of the coil so that straining occurred in the transverse direction of the coil (i.e., $\perp$ to the rolling direction). The blanks were 254 mm (10 in) wide and approximately 1067 mm (42 in) long. A 2.54 mm (0.1 in) diameter circle grid was electro-etched on the surface of the blanks to facilitate measurement of the strain. After forming, the channel sections were placed and stored on edge to avoid any modifications of the shape. Additional details regarding the procedure used to form the channel sections can be found in reference [16].
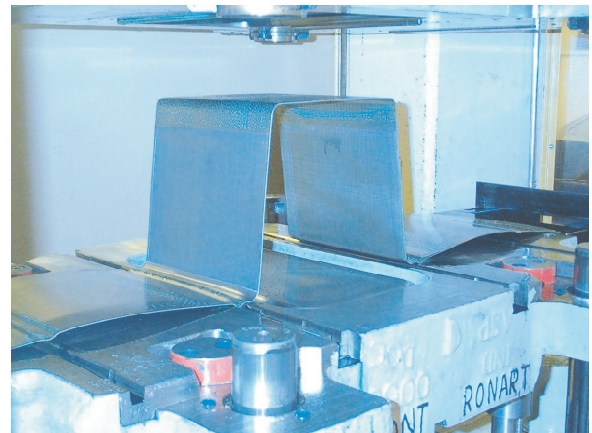

Figure 2: A channel section formed in the A/SP channel draw die (courtesy of IRDI).

Friction specimens with nominal dimensions of 30 mm x 80 mm were cut from the DQSK sheet stock in the as-received condition such that the long dimension of the specimen was orientated parallel to the rolling direction. Pre-strained specimens of the same geometry were also cut from sidewall sections of the pre-strained channel produced with a 100 % bead penetration. This condition generated an approximate strain level of 21.5 % in the sidewall section. (Note that the long dimensions of the

pre-strained specimens were in a perpendicular orientation to the strain direction.)

FRICTION EXPERIMENTS- A schematic diagram of the apparatus used to evaluate the friction behavior is shown in Figure 4. The apparatus was designed for use in conjunction with a high-speed, servo-hydraulic testing platform. As shown in the figure, the friction apparatus consists of an upper, mobile grip that is attached the actuator; and a lower, stationary grip frame that is attached to the load cell of the servo-hydraulic testing platform. One end of the test specimen is attached to the upper grip and the other is held between two 6.35 mm diameter ball indenters. Hardened tool steel balls were used for the indenters for two reasons: First, the force interactions between a flat sheet of a "soft" material and a hard spherical surface are well studied and many force models are available in the literature. Second, most of the dies used in automotive metal forming operations are machined from hardened steel. Using a similar material for the indenters will allow for examinations of any possible interactions between steel and the surfaces created during an experiment. The normal force was applied to the sample via the indenters and two small load cell/lever arm assemblies. The load cells that monitor the normal forces are mounted in the large, rigid steel supports of the stationary grip frame to eliminate any rotational, or side loading that could occur during the test.
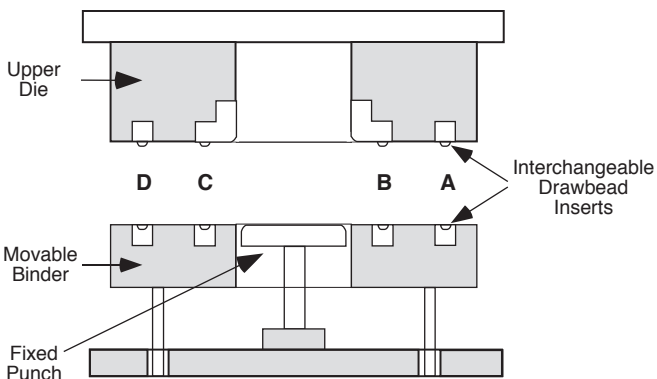

Figure 3: Sketch of the channel draw die with location of drawbead inserts (courtesy of IRDI).

The large pressure reservoirs in the servo-hydraulic testing platform produce immediate actuator motion at the pre-programmed displacement rate; making the time required to reach a steady-state velocity effectively zero. In addition, the actuator moved continuously under closed-loop position control at that displacement rate until the pre-determined endpoint was achieved. Thus, any variability in the applied load that could be transmitted to the specimen was effectively eliminated. The total displacement for these experiments was 12.5 mm (0.5 in) at a fixed displacement rate of 25.4 mm/s (1.0

in/s). The indentation forces used for these experiments were 500 N (112.4 lb$_f$) and 1250 N (281 lb$_f$). The friction behavior was evaluated under both unlubricated and lubricated conditions. Light paraffin oil was used as the lubricant for these experiments.

An experiment consisted of a minimum of three tests for each load/lubrication condition. A balanced indentation force was applied to the sample via the two load cell assemblies after which it was pulled through the indenters by a single continuous actuator displacement. The actuator motion at the test start triggered the computer-controlled digital data acquisition system. Once triggered, the system continuously acquired the outputs of the two normal force load cells, the stationary load cell, and the actuator position with a minimum sampling frequency of 50 MHz until the end of the test.
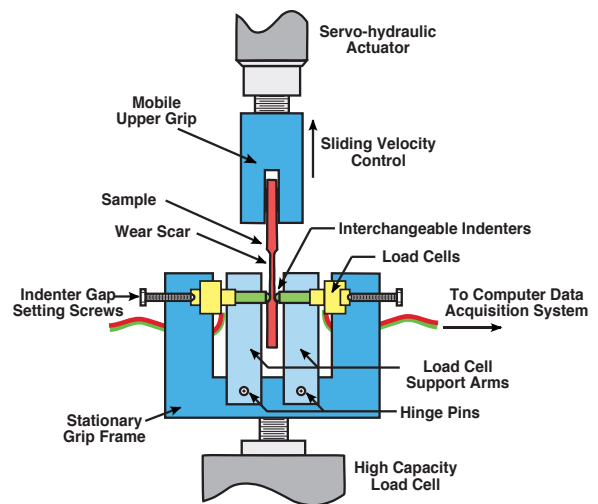

Figure 4. Schematic diagram of the prototype test apparatus used for the friction measurements.

SURFACE ROUGHNESS MEASUREMENTS- The topographies of both the initial surfaces and the wear scars created during the friction experiments specimen surface were examined with the SLCM. Details pertaining to the operation of the SLCM used for in study can be found in references [17-19]. All of the images in this analysis were created with a 635 nm laser optical source (λ), a 10x objective lens and a z-scan range of approximately 20 μm. These parameters generated intensity images of the surface with outstanding resolution and optical depth of field and with (x, y, z) dimensions of 1000 μm x 800 μm x 20 μm respectively. The spacing between the individual focal planes in each image was approximately 100 nm. Topographic maps were generated from the intensity images by the controlling software [17]. A series of linear roughness profiles with a typical length of 750 μm were collected from the topographic maps. Each profile contained a minimum of 2400 data points, resulting in an approximate sampling interval of 300 nm. A roughness measurement

consisted of a minimum of five, randomly placed profiles in the parallel orientation followed by five profiles in the perpendicular orientation with respect to the rolling direction of the sheet. Additional roughness measurements were performed along the length of the wear scars. These measurements consisted of several sequential 1000 μm profiles taken along a consistent feature in the scar.

RESULTS AND DISCUSSION

The results from a basic assessment of the initial surface roughness are shown in Table 1. The values in the table are averages of the measurements taken in the parallel and perpendicular directions. As expected, both the rms average roughness (Rq), the maximum peak height (Rmax) and the associated measurement uncertainty values are considerably larger for the pre-strained condition.

Table 1. Initial surface roughness of the DQSK steel

Surface Condition	Rq [μm]	Unc. [2σ]	Rmax [μm]	Unc. [2σ]
As-received	0.775	0.047	2.408	0.366
Pre-strained	1.527	0.222	4.719	0.726

A basic frictional force, **F**, can be defined for any loading situation as the force normal to an interface between two bodies that resists the motion produced by the action of an externally applied force [13, 14]. A dimensionless coefficient of friction, μ, can be defined from the basic frictional force as the ratio between the force required to produce movement and the normal force, **N**, that resists motion (i.e., $\mu = F/N$). This general definition can then be used to define both a coefficient of static friction (μ_s) from the force that is just sufficient to resist the onset of the relative motion (F_s) and a coefficient of sliding friction (μ_k) from the force that resists relative motion after sliding has initiated (F_k). As noted by Blau [14], these coefficients are simple quantities that only express the proportionality between two forces and, as noted earlier, all coefficients of friction are a function of the test parameters including sliding time, indentation force, strain rate, and the test environment.

An example of the typical friction behavior observed during the experiments is shown in Figure 5. Three distinct regimes are exhibited in this figure: the fully static (i.e., zero actuator velocity), the steady-state dynamic (i.e., sliding), and the transition between the static and dynamic regimes. In some literature accounts, the transition regime is referred to as the "run-in." However, this term generally describes the initial period where the surface roughness changes during sliding in a test where the same surfaces repeatedly slides over one another (e.g., a pin on disk test). Considering that this

test protocol consisted of a single-pull through the indenters, and that the surfaces interacted only once, "run-in" is not an appropriate term. Therefore, this section of the curve will be referred to as the "transient" regime.
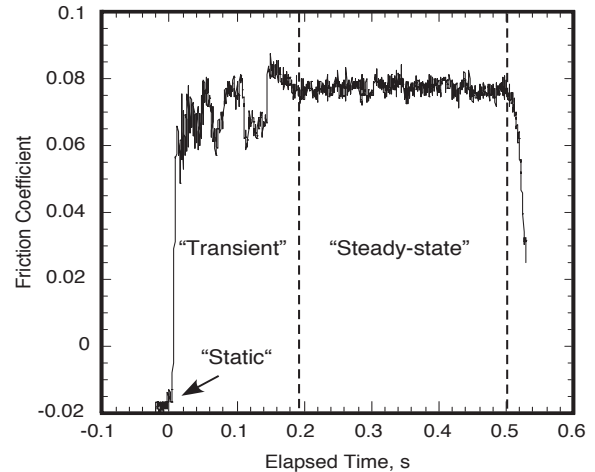

Figure 5. Variation in friction coefficient as a function of time for lubricated DQSK steel under a 1250 N indentation force.

A summary of an analysis of the friction data is presented as a function of the surface roughness condition in Table 2. Several friction parameters can be derived from a test of this type. For brevity, only the average normal force (**N**), the average coefficient of steady-state friction (μ_k) and the uncertainty associated with the friction coefficients are presented. Note that the average normal force values shown in the table are one-half the maximum indentation force. The basis for this being, the measured indentation force is actually the sum of the absolute values of the two equal and opposing normal forces acting on the surface of the specimen (i.e., $F_{ind} = 2 F_N$).

Overall, the results from this set of experiments appear to be reasonable with respect to the values reported in the literature for mild steel [3, 20-22]. The friction coefficients acquired from the tests in the unlubricated condition are somewhat higher than those acquired from the lubricated condition. Similarly, the coefficients acquired from the pre-strained surfaces are consistently higher than those acquired from the as-received surfaces. However, the friction coefficients at the two normal forces in the unlubricated pre-strained conditions are essentially the same. This implies that the steady-state friction coefficient may have become insensitive to the normal force for this lubrication/surface roughness condition. While the increase in the friction coefficients between the lubricated as-received and the lubricated pre-strained conditions might appear unusual, this trend also agrees

Table 2. Friction data obtained for DQSK steel.

As-received				Pre-strained			
Avg. N [N]	Lubricity	Avg. μ_k	Unc. [2σ]	Avg. N [N]	Lubricity	Avg. μ_k	Unc. [2σ]
250	None	0.0616	0.013	250	None	0.1135	0.012
625	None	0.0939	0.005	625	None	0.1110	0.010
250	Paraffin oil	0.0335	0.006	250	Paraffin oil	0.0614	0.002
625	Paraffin oil	0.0454	0.011	625	Paraffin oil	0.0698	0.007

with the literature. An increase in friction in the lubricated state can be attributed to several effects including interactions between bare surfaces (i.e., micro-scale galling) [23] as well as to the influence of localized variations in the hardness produced during bulk deformation that alter the fractional area of contact around the indenter [24, 25]. An additional source for this behavior may be the interactions between the steel indenter and the softer zinc coating on the surface. As a result, additional analyses are in progress to ascertain the relative influence of the zinc coating on the friction behavior of the DQSK steel.

Assessing the character of the roughness in the wear scar created during a friction experiment can be a challenging measurement. However, the linear wear track produced by this test methodology easily allows for detailed characterizations of the surfaces in the SLCM. The images shown in Figure 6 are topographies of a typical wear scar acquired from the DQSK steel (at a indentation load of 1250 N) by the SLCM. Figure 6a shows the surface conditions at the initiation of the test. The circle indicates the initial position of the indenter (i.e, the static regime in Figure 5) and the dashed lines reflect the evolution of the wear scar (i.e., the initial segment of the transient regime). Figure 6b shows the topography of the wear scar after the transient friction developed into the steady-state mode (i.e., the sliding regime). The solid line in both figures represents the location of the continuous surface roughness measurement taken along the length the wear scar with the SLCM. This measurement was created from a series of sequential topographic images taken along the length of the wear scar. The roughness profile at the maximum depth of the wear scar is shown in Figure 7. Note that while the total length of the scar was 12.5 mm, only the first 6.75 mm (i.e., 21,000 data points) are shown in this figure. The profile was cropped to accentuate the resolution of the closely spaced height variations that would have been suppressed had the entire profile been presented. The profile in Figure 7 consists of both the steady-state and the transient regimes and the transition appears to occur at approximately 2.8 mm. The dashed line in the figure indicates the transition point.
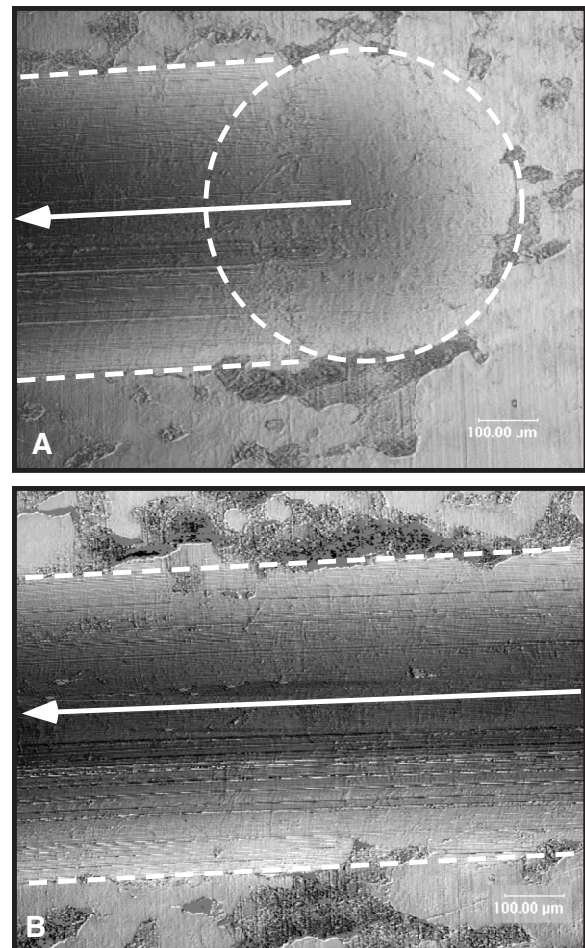

Figure 6. SLCM topographic images of the wear scar produced in lubricated DQSK steel under a1250 N indentation force.

Because this technique was intended to measure both the friction behavior and the roughness character in the wear scar at virtually any point during the test, it is then reasonable to determine whether any correlations exist between the features in the two profiles. While the behaviors in both the transient and the steady-state regimes have significance in a metal forming operation, sliding friction has been better characterized in the literature. With this in mind, it was appropriate to
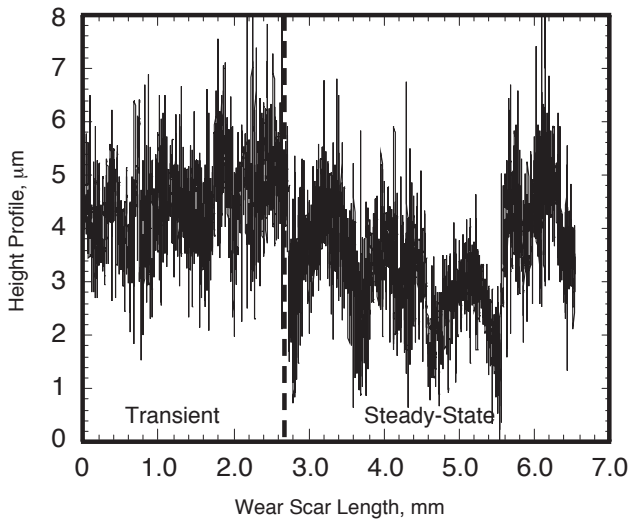
Figure 7. Corresponding roughness profile of the wear scar shown in Figure 6.
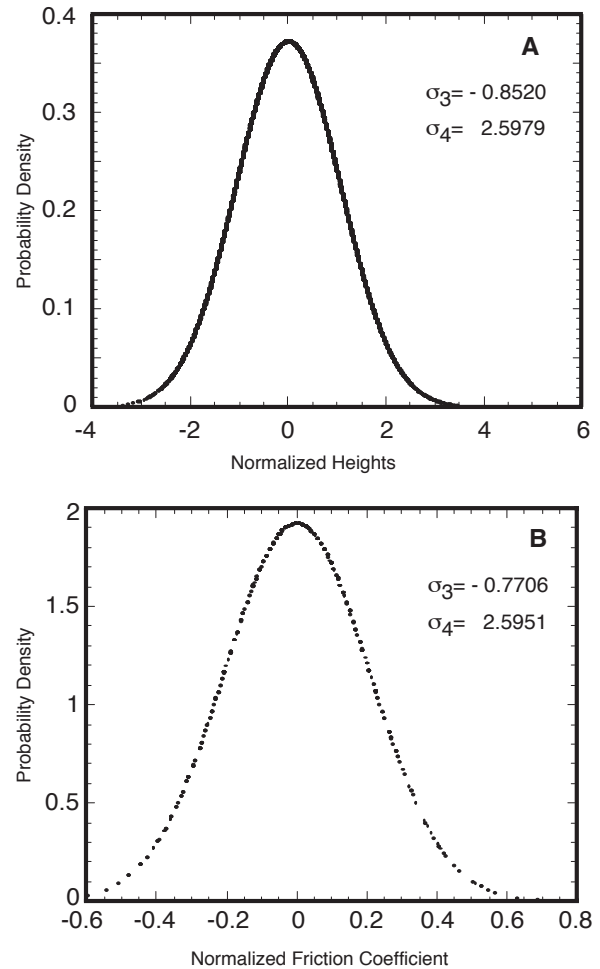

Figure 8. Probability density functions of the steady-state friction behavior. a) the surface roughness profile (Figure 7), b) friction coefficient (Figure 5).

surface roughness profile may produce larger variations in the contact area; and thereby, have a stronger influence on the friction than the mean roughness. This relationship does imply that a correlation may exist between the largest asperities present in the wear scar of the DQSK steel and the local maxima in the friction coefficient profile.

ascertain the degree of correlation in the steady-state regime. The large number of data points in the roughness profile required additional reduction to facilitate data manipulation. Thus, the roughness data was cropped to correspond with the friction data in the time interval between 0.25 s and 0.4 s (see Figure 5). A simple, straightforward analysis was performed to match both profiles to centered Gaussian distributions. This was achieved by fitting the data from the two profiles to a normal Gaussian probability density function in the same manner shown in references [19] and [26]. The results are presented in Figure 8. The PDF of the roughness data is shown as Figure 8a and the PDF of the force data is shown as Figure 8b. The two figures were plotted on different axes to accentuate the similarities between the two data sets. Had the data sets been plotted on the same set of axes, the range of the roughness data would have been compressed to the extent where these similarities would not be apparent. However, the quality of a Gaussian fit is characterized by the values of the higher central moments about the mean. The skew (σ_3) is a measure of the asymmetry in the overall shape of the distribution and the kurtosis (σ_4) characterizes the shape of the tails of the distribution. The ideal Gaussian shape is characterized by a skew (σ_3) of zero and by a kurtosis (σ_4) of three [27, 28]. The skew and kurtosis values for the roughness probability density function are −0.8520 and 2.5979 respectively, whereas the skew and kurtosis values for the friction probability density function are −0.7706 and 2.5951. The fact that the skew values for the two distributions are within 10 % of each other indicates that the general shapes of the distributions are quite similar. Furthermore, the kurtosis values are essentially identical which indicates that the extremes of the two distributions are closely related. Clearly, further analysis is required before any causal relationship can be established between these two distributions; but it has been suggested that the extremes in the distribution of a

CONCLUSION

A prototype test apparatus has been developed as part of a test protocol designed to address the need for friction measurements that provide a more broad-based understanding of the complex relationships between the friction behavior and the microstructural variations that affect the properties during metal forming. The principal advantage of this protocol is that it enables direct assessment of the relative influence of metallurgical variables, such as composition, grain size and orientation effects, strengthening mechanisms, slip homogeneity, as well as changes in the microstructures that are

produced under conditions closely emulating those encountered in industrial forming operations.

A series of single-pull friction experiments were conducted on hot-dipped DQSK steel under two normal forces, in two surface roughness conditions, and under two lubricities. The resulting surfaces were examined with the SLCM. The goal of this particular study was to determine whether this prototype measurement apparatus could produce friction data that are comparable to those obtained under actual automotive metal forming conditions, and enable detailed characterizations of the surfaces created under those experimental conditions.

The results demonstrated that:

• The friction coefficients calculated from the force data are within the range of values reported in the literature for steel. Considering that all friction coefficient data are dependent upon parameters used in the test, the reasonable agreement is an indication that the measurement sensitivity is appropriate for the intended purpose.

• The test apparatus can easily distinguish the transition from the static to the sliding state and that the magnitude of the friction coefficients can be determined in real time in the steady-state and in the transient friction regimes for any condition.

• The wear scars are suitable for detailed surface analysis in the SLCM. The linear shape of the wear scar facilitated detailed surface characterization in the SLCM. The combination of high-resolution topographic analysis and roughness measurements in the wear scar enabled a thorough assessment of the character of the surface asperities.

• The measurement sensitivity is such that the quality of the resulting data is amenable to detailed statistical analysis. A simple analysis of the distributions of the steady-state friction coefficient and the surface roughness of the wear scar in the same region revealed that a correlation could exist between the largest asperities and the local maxima in the friction coefficient profile.

Based on the results, it was concluded that the prototype successfully met the design criteria for the experimental technique and that the measurement protocol is appropriate for further development. As a result, a wide range of experiments are planned to further evaluate the influences of initial surface roughness, strain path and asperity distribution, indenter shapes, as well as indentation forces, strain rates and surface lubricants.

REFERENCES

1. J.A. Schey, in *Metal Deformation Processes- Friction and Lubrication*, J.A. Schey, Ed., New York, NY, Marcel Dekker Inc, 1970, pp. 15-81.

2. O. Mahrenholtz, N. Bontcheva, R. Iankov, and M. Datcheva, *Mech. Res. Comm.*, 2000, vol. 27 (4), pp. 393-402.

3. M.R. Lovell and Z. Deng, *Wear*, 1999, vol. 236, pp. 117-127.

4. M.Y. Demeri, *J. Mater. Eng. & Perf.*, 1993, vol. 2 (6), pp. 863-866.

5. M.R. Stoudt and R.E. Ricker, *Metall. Mater. Trans. A*, 2002, vol. 33A, pp. 2883-2889.

6. H. Naceur, Y.Q. Guo, J.L. Batoz, and C. Knopf-Lenoir, *Int. J. Mech. Sci*, 2001, vol. 43 (10), pp. 2407-2434.

7. L. Gunnarsson and E. Schedin, *J. Mater. Proc. Tech*, 2001, vol. 113 (2), pp. 168-173.

8. J. Cao, B.L. Kinsey, et al., *Robotics and Computer-Integrated Manufacturing*, 2001, vol. 17 (1-2), pp. 49-56.

9. P.K. Saha, W.R.D. Wilson, and R.S. Timsit, *Wear*, 1996, vol. 197, pp. 123-129.

10. W.R.D. Wilson, *J. Manu. Sci. & Engr.*, 1997, vol. 119, pp. 695-698.

11. S.W. Lo and T.C. Horng, *J. Tribology*, 1999, vol. 121, pp. 224-233.

12. H. Sofuglu, H. Gedikli, and J. Rasty, *J. Eng. Mat. Tech.*, 2001, vol. 123 (3), pp. 338-348.

13. F.P. Bowden and D. Tabor, *The Friction and Lubrication of Solids*, London, Oxford University Press, 1950.

14. P.J. Blau, *Friction Science and Technology*, New York, NY, Marcel Dekker, 1996.

15. N.P. Suh and H.C. Sin, *Wear*, 1981, vol. 69 (1), pp. 91-114.

16. D.E. Green, SAE Technical Paper 2001-01-1136., 2001.

17. M.R. Stoudt, J.B. Hubbard, S.A. Janet, and J. Liu, in *Trends in Materials and Manufacturing Technologies for Transportation Industries*, T. R. Bieler, J. E. Carsley, H. L. Fraser, and J.E. Smugeresky, Eds., Warrendale, PA, TMS, In Press.

18. M.R. Stoudt and J.B. Hubbard, *Submitted to Acta Materiala*.

19. M.R. Stoudt, J.B. Hubbard, and S.W. Banovic, in *SAE Special Publication #1837: Innovations in Modeling and Testing of Steel Structures for Automotive Applications*, R. Mohan, V.C. Shah, and J.G. Speer, Eds., Warrendale, PA, SAE, 2004.

20. A.J. Black, E.M. Kopalinsky, and P.L.B. Oxley, *J. Mech. Engr. Sci.*, 1993, vol. 207 (5), pp. 335-353.

21. D.A. Korzekwa, P.R. Dawson, and W.R.D. Wilson, *Int. J. Mech. Sci.*, 1992, vol. 34 (7), pp. 521-539.

22. M.R. Lovell, Z. Deng, and M.M. Khonsari, *J. Tribology*, 2000, vol. 122 (4), pp. 856-863.

23. J.A. Schey, *Tribology in Metalworking*, Metals Park, OH, ASM, 1983.

24. W.R.D. Wilson and W. Lee, *J. Manu. Sci. & Engr.*, 2001, vol. 123, pp. 279-283.

25. W.R.D. Wilson and S. Sheu, *Int. J. Mech. Sci.*, 1988, vol. 30 (7), pp. 475-489.

26. M.R. Stoudt, J.B. Hubbard, and S.W. Banovic, *SAE Trans. J. Mater. Manuf.*, In Press.

27. W. Mendenhall, *Introduction to Probability and Statistics*, 4th ed., N. Scltuate, MA, Duxbury Press, 1975.

28. W. Feller, *An Introduction to Probability Theory and its Applications*, vol. 2, 2nd ed., NY, NY, J. Wiley & Sons, 1971.

CONTACT

Mark. R. Stoudt, Steven P. Mates, and Joseph B. Hubbard- Materials Performance Group, Materials Science and Engineering Laboratory. Email: mark.stoudt@nist.gov, steven.mates@nist.gov, joseph.hubbard@nist.gov.

Daniel E. Green, Assistant Professor, Mechanical, Automotive & Materials Engineering Department, University of Windsor. dgreen@uwindsor.ca.

DEFINITIONS, ACRONYMS, ABBREVIATIONS

A/SP: Automotive/Steel Partnership

DQSK: Draw Quality, Semi-Killed Steel

FEA: Finite Element Analysis

IRDI: Industrial Research & Development Institute

N: Normal Force equal to the (Indentation Force /2) in Newtons

PDF: Probability Density Function

SLCM: Scanning Laser Confocal Microscope

Rq: Root Mean Squared (rms) Roughness

Rmax: The maximum peak height in a roughness profile.

UNC: The statistical uncertainty equal to 2 standard deviations (σ) of the mean.

λ: Wavelength of the laser source in the SLCM.

μ_k: Coefficient of Steady-state (Dynamic) Friction (dimensionless)

σ_3: (Skew) A measure of the symmetry of the PDF.

σ_4: (Kurtosis) A measure of the shape of the tails of the PDF.